Eddy Trains and Striations in Quasigeostrophic Simulations and the Ocean

CHANGHENG CHEN[a] AND IGOR KAMENKOVICH

Rosenstiel School of Marine and Atmospheric Science, University of Miami, Miami, Florida

PAVEL BERLOFF

Department of Mathematics, Imperial College London, London, United Kingdom

(Manuscript received 18 March 2016, in final form 7 July 2016)

ABSTRACT

This study explores the relationship between coherent eddies and zonally elongated striations. The investigation involves an analysis of two baroclinic quasigeostrophic models of a zonal and double-gyre flow and a set of altimetry sea level anomaly data in the North Pacific. Striations are defined by either spatio-temporal filtering or empirical orthogonal functions (EOFs), with both approaches leading to consistent results. Coherent eddies, identified here by the modified Okubo–Weiss parameter, tend to propagate along well-defined paths, thus forming "eddy trains" that coincide with striations. The striations and eddy trains tend to drift away from the intergyre boundary at the same speed in both the model and observations. The EOF analysis further confirms that these striations in model simulations and altimetry are not an artifact of temporal averaging of random, spatially uncorrelated vortices. This study suggests instead that eddies organize into eddy trains, which manifest themselves as striations in low-pass filtered data and EOF modes.

1. Introduction

Observations of quasi-zonal jetlike structures (striations) in the world's oceans enriched our understanding of the oceanic general circulation (Maximenko et al. 2005; Maximenko et al. 2008; Buckingham et al. 2014). Typical zonal velocities of these striations alternate with latitude and are on the order of $O(1)\,\mathrm{cm\,s^{-1}}$. With such strength, they contribute significantly to the low-frequency component of the flow. The presence of long correlation length scales also contributes to the anisotropy of eddy-induced material transport, which may have important implications for tracer distributions (Kamenkovich et al. 2015).

Although some components of the alternating striations can be stationary, they are mostly time-dependent features. The temporal variability of these features can be difficult to quantify because of both the significant variability of the large-scale circulation and the lack of long-term observations needed for reliable statistics. In particular, the striations drift meridionally, and the causes of this drift are not clear. Chen and Flierl (2015) showed that striations can be advected meridionally by meridional background flows. Drifting quasi-zonal jets were observed in a flow with a constant zonal topographic slope (Boland et al. 2012) and in the vicinity of isolated topographic ridges (C. Chen et al. 2015). It is, therefore, possible that the meridional drift is closely associated with the zonal component of the mean potential vorticity gradient (K. Srinivasan 2014, personal communication).

Unlike the strong, stationary jets in planetary atmospheres (Kondratyev and Hunt 1982), these striations are only visible after the application of low-pass filtering in time, which is intended to remove ambient mesoscale variability. This property makes the interpretation of striations challenging. Several idealized numerical studies described these oceanic jets as coherent jet flows (e.g., Richards et al. 2006; Baldwin et al. 2007; Berloff et al. 2011), an analogy of the jet streams in planetary atmospheres (Kondratyev and Hunt 1982). Schlax and Chelton (2008) suggested that the striations can instead

[a] Current affiliation: Department of Systems Design Engineering, University of Waterloo, Waterloo, Ontario, Canada.

Corresponding author address: Changheng Chen, Department of Systems Design Engineering, University of Waterloo, 200 University Avenue West, Waterloo ON N2L 3G1, Canada.
E-mail: cchen@rsmas.miami.edu

DOI: 10.1175/JPO-D-16-0066.1

be a pure artifact of insufficiently long time averaging of zonally propagating, isolated, random eddies. Such eddies are referred to as "random" because their position and propagation paths are not spatially correlated between each other and do not correspond to any large-scale pattern. R. Chen et al. (2015) demonstrated that the low-frequency components of nondispersively propagating eddies can indeed manifest themselves as jets. However, Buckingham and Cornillon (2013) found that a significant portion of the time-mean striations is inconsistent with the spurious jets proposed by Schlax and Chelton (2008).

In summary, there are at least three interpretations of the oceanic jets in literature: 1) as distinct, coherent components of the flow embedded in an eddy field (e.g., Richards et al. 2006; Baldwin et al. 2007; Berloff et al. 2011), 2) as an artifact of time averaging of random eddies (Schlax and Chelton 2008), and 3) as coherent flows with strong contributions from eddies (Buckingham and Cornillon 2013; R. Chen et al. 2015). In this study, we use the term striations to describe the quasi-zonal structures obtained from low-pass filtering of observational and model data and demonstrate that the striations arise from systematically propagating "eddy trains," which we define as a series of compact cyclones and anticyclones propagating along alternating paths or tracks. These eddy trains are an intrinsic, low-frequency component of the baroclinic, double-gyre circulation (see also Kamenkovich et al. 2009b) and do not require external forcing as in previous studies (O'Reilly et al. 2012). These eddy trains are contrasted with "random eddies." The distinction is important because the existence of eddy trains' striations imply the existence of dynamical mechanisms that set these large-scale templates for eddy propagation, whereas generation of random eddies can be purely local.

To shed light on the nature of the striations and their relationship to eddies, we study their properties in a hierarchy of progressively more realistic oceanic flows. First, we study a quasigeostrophic (QG) channel model driven by an imposed, horizontally uniform, vertically sheared flow, which is intended as an illustration of stationary eddy trains. Our main focus is on the drifting eddy trains in the subtropical gyres first in a wind-driven QG model of midlatitude double gyres and then in altimetry data. Past studies investigated striations in double-gyre settings but did not focus on the role of baroclinic eddies (Nadiga 2006; Tanaka and Akitomo 2010; O'Reilly et al. 2012).

This paper is structured in the following way: Section 2 introduces the two QG models, the altimetry data, and the methods for identifying coherent eddies and low-frequency striations. Section 3 explores eddy trains and striations in a channel model. Section 4 studies nonstationary (migrating) striations and eddy trains in a wind-driven, double-gyre model. Section 5 applies the results from the model simulations to interpret the relationship of coherent eddies and striations in the altimetry data. Conclusions are given in section 6.

2. Models, data, and methods

a. The models

1) The QG channel model

The first model of striations and eddies used here is a two-layer QG channel model on the β plane, which can be considered as an idealized Antarctic Circumpolar Current (ACC). The main purpose of this simulation is to illustrate the concept of an eddy train in the regime where these structures are stationary and straightforward to define. The meridional width of the channel is $L_y = 3600\,\mathrm{km}$, and the channel is zonally periodic with the period $L_x = L_y$. The grid resolution is about $7\,\mathrm{km} \times 7\,\mathrm{km}$. The Coriolis parameter f_0 is $0.83 \times 10^{-4}\,\mathrm{s}^{-1}$, and the planetary vorticity gradient β_0 is $2 \times 10^{-11}\,\mathrm{m}^{-1}\,\mathrm{s}^{-1}$. The stratification is defined by the depths of the top and bottom layers, $H_1 = 1\,\mathrm{km}$ and $H_2 = 3\,\mathrm{km}$, and the internal Rossby deformation radius is 25 km. The bottom friction parameter γ is $10^{-7}\,\mathrm{s}^{-1}$, and the eddy viscosity coefficient ν is $10\,\mathrm{m}^2\,\mathrm{s}^{-1}$. These parameters are chosen to produce multiple zonal jets that are "latent," that is, weaker than the eddy field, which is most relevant to midlatitude oceans (Kamenkovich et al. 2009b; Berloff et al. 2011).

There is a uniform zonal background flow of $6\,\mathrm{cm\,s}^{-1}$ in the upper layer, and the lower layer has no background flow. The vertical shear of the background flow is supercritical and leads to the development of baroclinic instability and subsequent generation of eddies and striations (Berloff et al. 2009). A more detailed description of this model can be found in Berloff et al. (2009).

2) The double-gyre QG model

The three-layer, double-gyre, QG model simulates wind-forced circulation in a closed-ocean basin on the β plane (Karabasov and Goloviznin 2009; Berloff 2015). Potential vorticity (PV) q_n in each of the three layers is governed by

$$\frac{\partial q_n}{\partial t} + J(\varphi_n, q_n) = \delta_{n1}\mathcal{F} + \nu\nabla^4\varphi_n - \delta_{n3}\gamma\nabla^2\varphi_n \quad (n = 1, 2, 3), \tag{1}$$

where the layer index starts from the top, φ_n are streamfunction disturbances, $J(\cdot, \cdot)$ is the Jacobian operator, δ is

the Kronecker delta, $\nu = 100\,\mathrm{m^2\,s^{-1}}$ is the eddy viscosity coefficient, $\gamma = 10^{-7}\,\mathrm{s^{-1}}$ is the bottom friction parameter, and $\mathcal{F}$ is the surface Ekman pumping with an asymmetric, double-gyre shape (Berloff 2015).

The stratification parameters of this model are as follows:

$$F_1 = \frac{f_0^2}{g_1' H_1}, \quad F_{21} = \frac{f_0^2}{g_1' H_2}, \quad F_{22} = \frac{f_0^2}{g_2' H_2}, \quad F_3 = \frac{f_0^2}{g_2' H_3}, \tag{2}$$

where $f_0 = 0.83 \times 10^{-4}\,\mathrm{s^{-1}}$ is the Coriolis parameter, g'_n are the reduced-gravity coefficients associated with the density jump between the layers, and $H_n = 250$, 750, and 3000 m are the depths of the three layers from top to bottom. The stratification parameters are set in such a way that the first and second Rossby deformation radii are 30.7 and 14.2 km. The Rossby deformation parameters are $F_1 = 1.55 \times 10^{-9}\,\mathrm{m^{-2}}$, $F_{21} = 5.16 \times 10^{-10}\,\mathrm{m^{-2}}$, $F_{22} = 1.47 \times 10^{-9}\,\mathrm{m^{-2}}$, and $F_3 = 3.69 \times 10^{-10}\,\mathrm{m^{-2}}$. The isopycnal PV q_n is related to the streamfunction perturbations via PV inversion:

$$\begin{aligned} q_n = {} & \nabla^2 \varphi_n + \beta_0 y + \delta_{n1} F_1 (\varphi_2 - \varphi_1) \\ & + \delta_{n2} [F_{21}(\varphi_1 - \varphi_2) + F_{22}(\varphi_3 - \varphi_2)] \\ & + \delta_{n3} F_3 (\varphi_2 - \varphi_3), \end{aligned} \tag{3}$$

where $\beta_0 = 2 \times 10^{-11}\,\mathrm{m^{-1}\,s^{-1}}$ is the planetary vorticity gradient.

The basin is a 3840 km × 3840 km square discretized with 513 × 513 grid points, so that the grid resolution is 7.5 km × 7.5 km. Figure 1 shows a sketch of the model. The effective advection scheme implemented in this model allows us to achieve large Reynolds numbers on relatively coarse grids (Karabasov et al. 2009).

b. Altimetry data

The focus of our analysis is on nonstationary (drifting) striations and propagating eddies. We therefore use the "all satellites merged" version of the delayed time maps of daily sea level anomaly (SLA) distributed by Archiving, Validation, and Interpretation of Satellite Oceanographic data (AVISO). The SLA is computed with respect to a 20-yr mean (1993–2012) and is interpolated on ¼° × ¼° grids. Zonal and meridional near-surface geostrophic velocity anomalies can be found from the SLA h according to

$$u = -\frac{g}{f}\frac{\partial h}{R\partial\phi}, \quad v = \frac{g}{f}\frac{\partial h}{R\cos\phi\partial\lambda}, \tag{4}$$

where R is the radius of Earth, ϕ is latitude, and λ is longitude. We detect coherent eddies and striations from u and v with the modified Okubo–Weiss parameter and spatiotemporal filtering techniques, respectively.

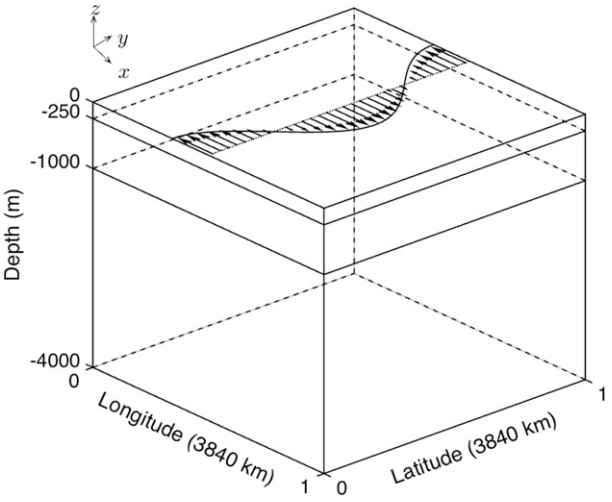

FIG. 1. Sketch of the three-layer, double-gyre, QG model with an asymmetric wind curl forcing (arrows) at the top layer.

c. Detection of the cores of coherent eddies

To study the relationships between striations and eddies, we first introduce a new parameter to detect the cores of coherent eddies in eddying flows. Okubo (1970) and Weiss (1991) introduced the Okubo–Weiss parameter to detect and describe eddying flow:

$$Q^2 = S^2 - \omega^2, \tag{5}$$

where $S^2 = (\partial u/\partial x - \partial v/\partial y)^2 + (\partial v/\partial x + \partial u/\partial y)^2$ is the squared horizontal strain rate, and $\omega^2 = (\partial v/\partial x - \partial u/\partial y)^2$ is the squared vertical vorticity component. Negative values of Q^2 correspond to a vorticity-dominated flow, such as the cores of vortices, while positive values suggest that the flow is strain dominated, as it often happens outside of the vortex cores. We define a "modified Okubo–Weiss parameter" based on Q^2:

$$E^2 = \frac{\omega}{2|\omega|}(|Q^2| - Q^2), \tag{6}$$

which equals $\pm|Q^2|$ when $Q^2 < 0$ and is zero otherwise. Positive/negative values of E^2 correspond to cyclonic/anticyclonic eddies; E^2 captures only the cores of strong, coherent eddies and excludes other transient features, such as meanders; weak, wavelike eddies; and transient striations. Figure 2a shows a cross section of an anticyclonic Gaussian eddy, and the corresponding E^2 parameter; this parameter is nonzero only within the vortex core, which overlaps the vortex part circled by the extremum of the rotational speed. This E^2 parameter is based on rotation and fluid deformation,

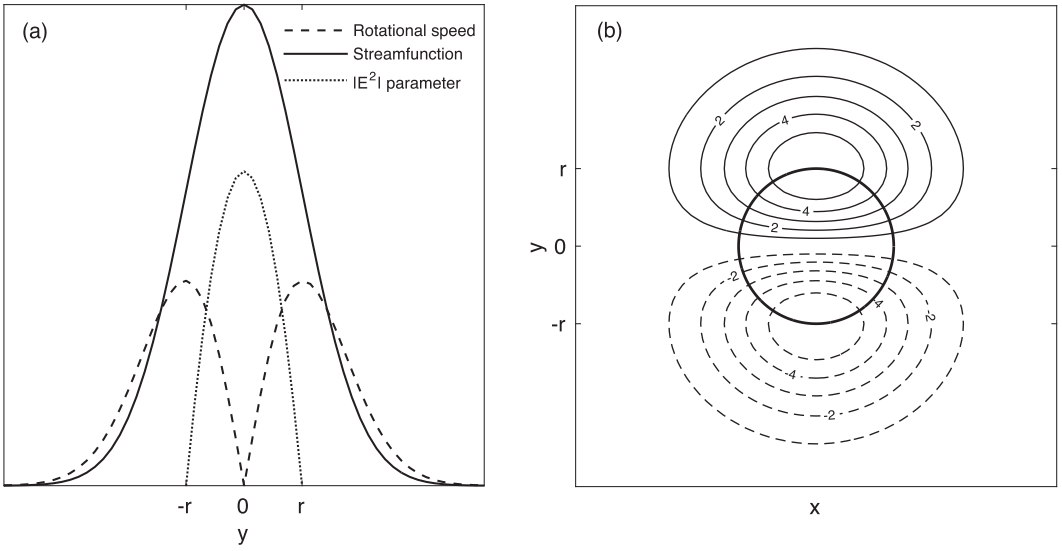

FIG. 2. Sketch of an anticyclonic Gaussian eddy: $\exp[-(x^2 + y^2)/(2r^2)]$. (a) The solid curve is the profile of its streamfunction at $x = 0$, $\exp[-y^2/(2r^2)]$; dashed curve is the rotational speed $|-y/r^2 \exp[-y^2/(2r^2)]|$; and dotted lines are the absolute value of the corresponding E^2 parameter, which is negative for anticyclonic eddies. (b) The corresponding zonal velocity of the eddy $y/r^2 \exp[-(x^2 + y^2)/(2r^2)]$, solid curves represent positive velocity and dash curves negative velocity, and the velocity values are arbitrary; the E^2 parameter is nonzero within the solid black circle, and the zonal velocity of the eddy within this circle only accounts for about 20% of its total zonal velocity.

unlike some other techniques that emphasize eddy material transport (e.g., Beron-Vera et al. 2013; Wang et al. 2015). A comparison of different methods on identifying mesoscale eddies can be found in Faghmous et al. (2015).

In the following sections, we use locations of the vortex cores to study propagation paths of cyclones and anticyclones. If these paths nearly coincide for several eddies, we call this chain of eddies an eddy train; E^2 cannot, however, be used to accurately estimate the velocity contribution from coherent eddies to striations, since it only accounts for the eddy cores (Fig. 2b); accurate definition of vortex boundaries are not straightforward and will not be attempted here. Based on the Gaussian eddy example considered here (Fig. 2a), we estimate that an eddy core defined this way corresponds to only approximately 25% of the corresponding eddy.

d. Degree of anisotropy for the detection of striations

Isolating striations, either from observational data or realistic numerical simulations, usually requires low-pass filtering. For example, Maximenko et al. (2005) discovered nonstationary zonal jets from a temporally filtered (18-week mean) sea level anomaly, while Maximenko et al. (2008) found zonally elongated, stationary striations from spatially filtered (two-dimensional Hanning filter of 4° half-width) mean dynamic topography (12-yr mean); Buckingham and Cornillon (2013) described zonally elongated striations from temporally (4-yr mean) and spatially high-pass filtered absolute dynamic topography. However, there is no consensus on how to choose an appropriate filtering time scale. Definition of striations can be very sensitive to this choice because too short a time scale can fail to filter out the eddies and too long an average can smear off nonstationary striations. In this study, we choose this time scale in an objective way by adapting the "degree of anisotropy" parameter:

$$\alpha = \frac{\langle u^2 \rangle - \langle v^2 \rangle}{\langle u^2 \rangle + \langle v^2 \rangle}, \tag{7}$$

which has been used to study zonality of flow fields (e.g., Shepherd 1990; Huang et al. 2007). Here, $\langle \cdot \rangle$ stands for area averaging and u and v stand for geostrophic velocity anomalies. When α varies from -1 to 1, then the flow varies from purely meridional to purely zonal. To define a new parameter γ that measures both the strength and zonality of the striations, we multiply α with the magnitude u:

$$\gamma = \frac{\overline{|\overline{u}^{x}|}^{y}}{u_0} \cdot \alpha, \tag{8}$$

where u_0 is a reference velocity and is chosen to be $1\,\mathrm{cm\,s^{-1}}$, $^{-x}$ and $^{-y}$ denote zonal and meridional averages, respectively, and $|\cdot|$ is the absolute value symbol.

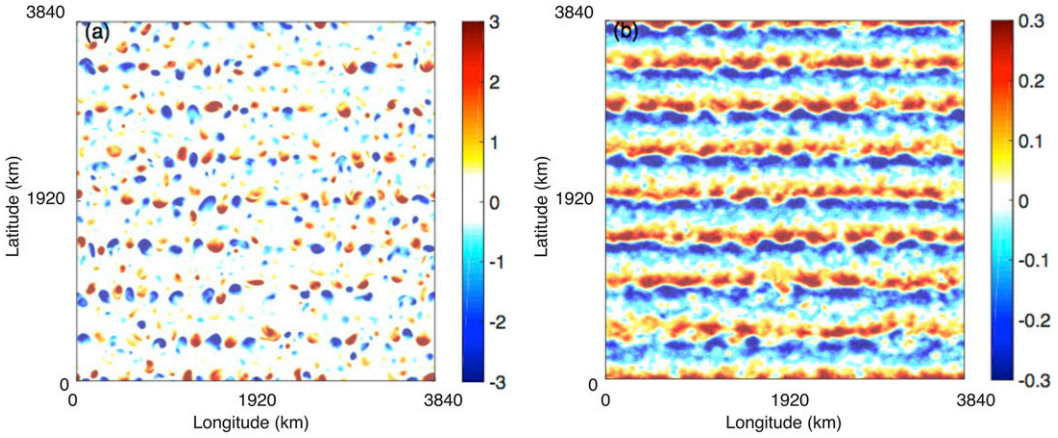

FIG. 3. The E^2 parameter (s^{-2}) for barotropic coherent eddies in the channel model: (a) snapshot and (b) 10-yr mean. Solid red dots in (a) represent the cores of cyclonic eddies, and solid blue dots represent the cores of anticyclonic eddies.

Essentially, γ defines the degree of zonality and strength of the flow in the area of interest; the larger the parameter γ, the more zonal and powerful is the flow. Note that the horizontal tilts of the quasi-zonal striations in this study are small; thus, we can determine the optimal time filtering scale for finding robust zonal striations by maximizing the value of γ.

3. Stationary striations and eddy trains in the zonal flow

Zonal QG flow on the β plane is baroclinically unstable when its vertical shear exceeds the critical shear (Pedlosky 1987), and the baroclinic instability leads to the formation of mesoscale features, such as mesoscale eddies and zonal striations (e.g., Berloff et al. 2009). Here, we investigate the relationship between coherent eddies defined by the E^2 parameter and striations detected from spatiotemporal filtering techniques as a stepping stone toward understanding their relationship in a more realistic wind-driven, double-gyre flow and, ultimately, in the altimetry data.

Zonal striations with velocity alternating with latitude characterize the flow in the channel. These features are stationary, unlike the drifting striations in more complex flows considered in the next section (see also Kamenkovich et al. 2009b). Very long time averages of this flow produce consistent zonal striations, and it is clear that they cannot be explained by propagating random eddies. To quantify the anisotropy of the striations and its dependence on the finite-time filtering scale, we calculate the anisotropy parameters α and γ for the barotropic component of the flow. The results are very similar for the baroclinic flow. As the time filtering scale increases, α and γ both increase dramatically from 0.18 and 0.34 and reach peak values of about 0.98 and 2.41, respectively, when the time scale is about 8.8 yr; afterward, α and γ remain almost constant. Thus, by choosing a time scale longer than 9 yr, we obtain relatively strong and zonal striations.

We find that coherent eddies defined by E^2 organize into eddy trains and propagate westward. Cyclonic and anticyclonic eddies are observed in pairs and propagate along alternating latitudes (Fig. 3a), thus forming zonally oriented cyclonic and anticyclonic eddy trains. Stray eddies are present as well and fall into the category of random eddies. Figure 4b is a

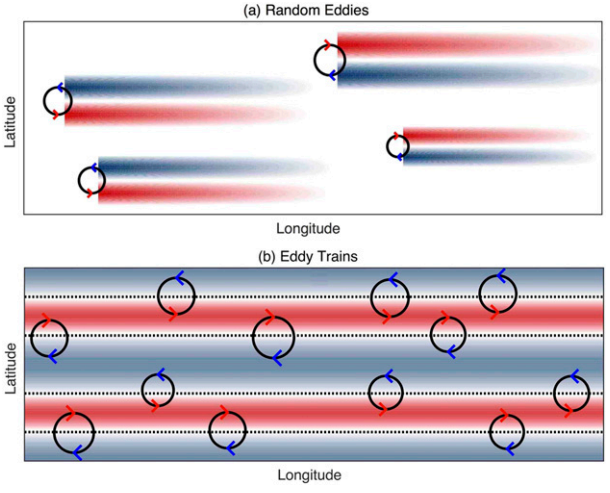

FIG. 4. Two scenarios of the relationship between eddies and striations: (a) striations being the artifacts of time averaging of propagating random eddies and (b) propagating eddy trains along four adjacent paths (dashed lines) leading to the emergence of striations in time-averaged fields. Each circle represents a cyclonic eddy or an anticyclonic eddy differentiated by the arrow directions, and red (blue) arrows indicate eastward (westward) speeds.

TABLE 1. Statistics of correlation coefficients between u_{eddy} and u_{total} and of the contribution from u_{eddy} to u_{total} from the Student's t test with a confidence level of 99%.

	Sample size	2D correlation[a]	1D correlation[b]	Ratio (%)[c]
QG channel model	25	0.85 ± 0.01[d]	0.95 ± 0.01	45.9 ± 0.4
Double-gyre QG model	100	0.86 ± 0.01	0.95 ± 0.01	42.8 ± 0.7
Sea level anomaly	1000	0.87 ± 0.001	0.96 ± 0.002	42.3 ± 0.1

[a] Correlation coefficient between u_{eddy} and u_{total}.
[b] Correlation coefficient between zonally averaged u_{eddy} and u_{total}.
[c] Ratio between area-averaged $|u_{eddy}|$ and $|u_{total}|$.
[d] $\mu \pm$ CI, where μ is the mean and CI is the confidence interval.

schematic of this scenario. The 10-yr average of E^2 also shows preferred steady paths for the eddy trains, which manifest themselves as multiple pairs of zonal bands (Fig. 3b). The band consisting of cyclonic eddies is always shifted to the north, and the boundaries between the paired bands correspond to eastward striations. The path of each eddy train is parallel to the striation axis. This is consistent with Berloff and Kamenkovich (2013b), who demonstrated that some eddies preferentially straddle eastward striations and maintain them via time-mean eddy forcing. Note that the latitudes of these paths are constant in time, and these are the examples of stationary (nondrifting) eddy trains.

To examine the contribution of the eddy trains to the striations, we next compare the zonal velocity of the striations u_{total} and that associated with the cores of coherent eddies u_{eddy}; u_{total} is the low-pass filtered zonal velocity, and u_{eddy} is calculated by accounting for velocities in vortex cores, where E^2 parameter is nonzero. We present the statistics of u_{eddy} and u_{total} by carrying out the Student's t test with the confidence level of 99% for 25 samples, each of which consists of flow snapshots covering a 10-yr period. First, u_{total} and u_{eddy} are strongly spatially correlated. The mean of their two-dimensional spatial correlation is 0.85 with a confidence interval (CI) of 0.01, and the mean correlation between their zonal averages is 0.95 with a CI of 0.01. Second, u_{eddy} contributes significantly to u_{total}. The mean percentage of u_{total} due to u_{eddy}, defined as the ratio between area-averaged $|u_{eddy}|$ and $|u_{total}|$, is 45.9% with a CI of 0.4%. The results are summarized in Table 1. We remind the reader that because of its definition, u_{eddy} underestimates the total contribution of vortices to the striations (see section 2c), and the net eddy effect is significantly larger. Although the shape of eddies is likely to be different from Gaussian, we will, nevertheless, assume that a ratio between $|u_{eddy}|$ and $|u_{total}|$ of more than 25% suggests a significant contribution of eddies to striations.

In summary, eddies in the channel model propagate along fixed paths, which we refer to as eddy trains. Time averages of the eddy trains contribute to stationary striations.

4. Nonstationary striations and eddy trains in the double-gyre flow

In this section, we examine the existence of striations and study their relations to coherent eddies in the baroclinic, wind-driven, double-gyre model. The instantaneous flow is composed of a double-gyre circulation, a meandering midlatitude jet, and ubiquitous mesoscale eddies (Fig. 5a). The asymmetry in the wind stress curl results in a slanted midlatitude jet, meandering northeastward. The double gyre weakens below the top layer, while the mesoscale eddies have a significant barotropic component and dominate the circulations in the deep layers.

Another distinct flow feature—nearly zonal, alternating striations embedded in the gyres—is clearly seen in the 1-yr mean barotropic streamfunction (figure not shown) and its corresponding velocity field (Fig. 5b). The striations are most distinct in the eastern parts of the domain, where the background flow is weak and predominantly nonzonal. Time averages over very long time (e.g., longer than 10 yr) do not show striations, since the striations are nonstationary and the long-term mean smears their signature. This property sets the striations apart from those in the zonal channel flow discussed above. Another possible scenario could be that these striations are artifacts of zonally propagating random eddies, but our analysis in section 4c disproves this.

Striations from the channel model are stationary; therefore, long time averaging is the best way to detect them. Nonstationary striations in the double gyres require more delicate definition that preserves their low-frequency variability. We first use spatiotemporal filtering to define these striations and study their main properties. These insights will help us to propose a

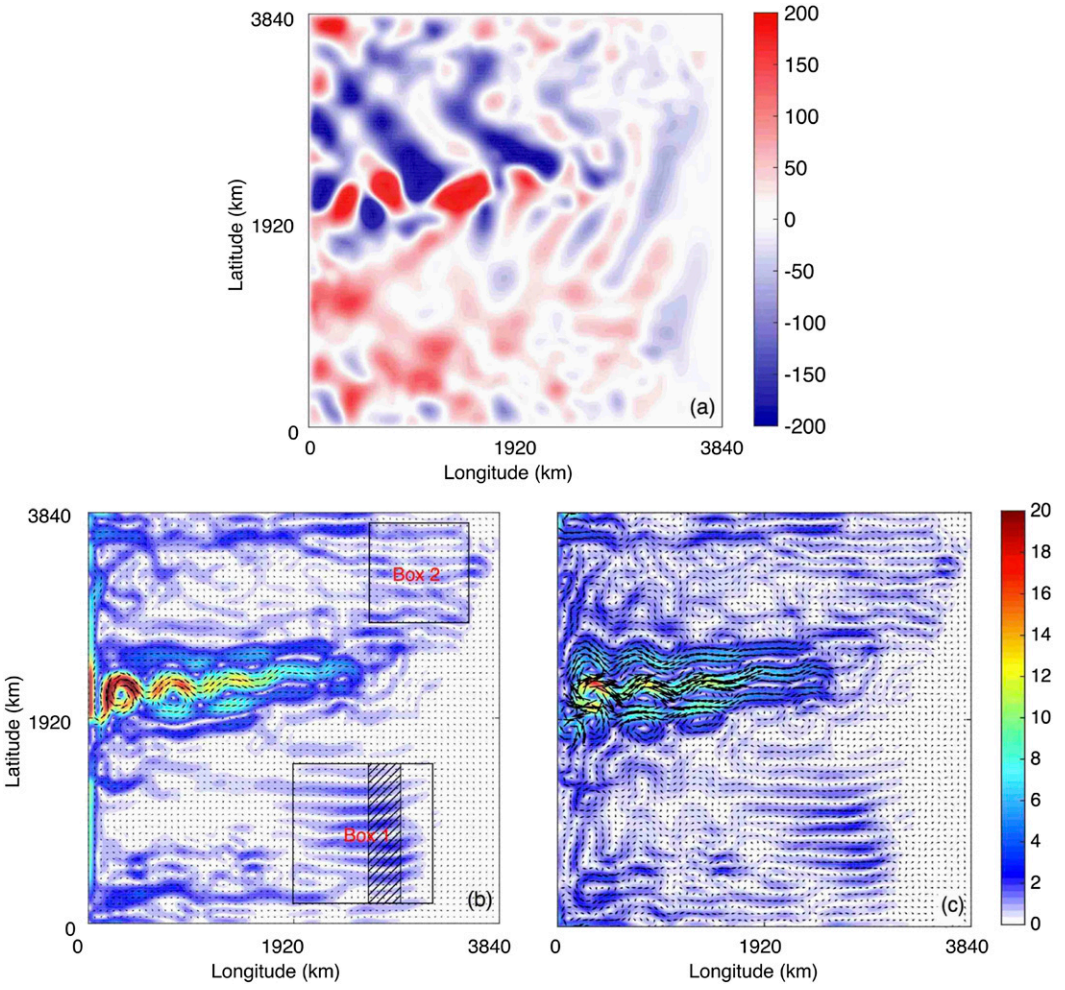

FIG. 5. Striations from spatiotemporal filtering: (a) instantaneous barotropic streamfunction ($m^2 s^{-1}$), (b) time-filtered (1-yr mean) barotropic velocity, and (c) barotropic velocity after spatial filtering applied to the flow in (b). The flows within the striped region, boxes 1 and 2 in (b), are selected to study eddy and striation properties (see text). Velocity magnitude is shown in shades and directions in arrows, and the velocity unit is $cm\,s^{-1}$.

better definition based on the empirical orthogonal function (EOF) method.

a. Nonstationary striations in the double-gyre flow

1) DETECTION OF STRIATIONS BY SPATIOTEMPORAL FILTERING

To determine the optimal averaging interval T_{aver} for the striations, we maximize the value of γ. We vary T_{aver} from 1 week to 10 yr and analyze the changes in the anisotropy parameters (section 2d) in the subpolar and subtropical rectangular regions (box 1 and box 2 in Fig. 5b); $\overline{|\overline{u}^x|}^y/u_0$ and α first increase with T_{aver}, which means that the low-pass filtered flow becomes more zonal and more powerful. For longer T_{aver}, $\overline{|\overline{u}^x|}^y/u_0$ and α decrease significantly because of the smearing of drifting striations. The maximum value of γ is attained at around T_{aver} of ~50 weeks for box 1 and of ~53 weeks for box 2; therefore, we choose 1 yr as our standard T_{aver} (Fig. 5b shows the corresponding striations).

This T_{aver} roughly corresponds to the vortex propagation time along the striation (Fig. 5b). For example, a vortex propagating zonally at the speed of $0.1\,m\,s^{-1}$ will travel over about 1500 km in T_{aver}. This analysis alone cannot, therefore, distinguish between eddy trains and random eddies. This distinction is quantified by our EOF analysis below.

To further isolate the nonstationary striations shown in Fig. 5b from the rest of the low-frequency variability

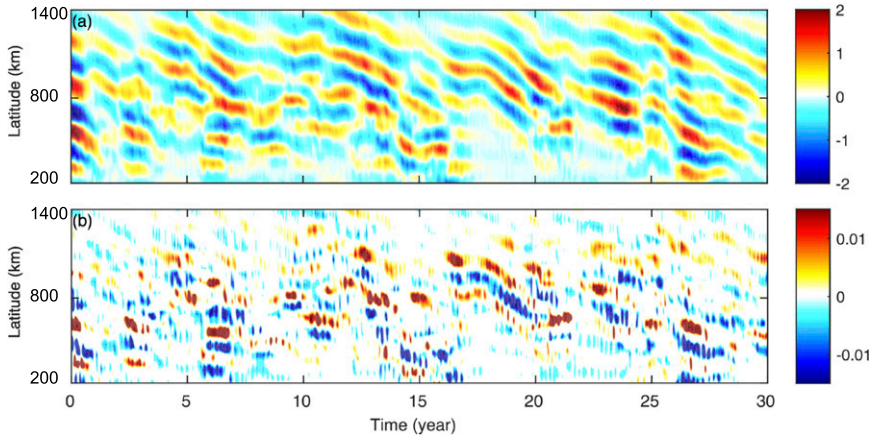

FIG. 6. Hovmöller diagrams of (a) a 1-yr mean zonal velocity ($\mathrm{cm\,s^{-1}}$) of the barotropic striations in the double-gyre flow and (b) the corresponding E^2 parameter ($\mathrm{s^{-2}}$) at the central longitude of box 1.

in the flow, we apply a high-pass spatial filter in the meridional direction. For this purpose, we calculate the ''wavenumber spectrum,'' which is the power spectrum density of the time-filtered barotropic streamfunction corresponding to Fig. 5b. The results for the full streamfunction in each isopycnal layer are quantitatively similar. A dominant peak around $k = 0$ and meridional wavelength of half the basin width shows up in the spectrum (figure not shown). This peak corresponds to the double-gyre, large-scale flow. We therefore choose a high-pass Fourier filter in the meridional direction with a cutoff wavenumber of 2 that excludes the double-gyre peak as discussed above and apply it to the 1-yr mean barotropic streamfunction. This application further accentuates the presence of zonal striations (Fig. 5c). The most significant difference between the flows in Figs. 5b and 5c is in the midlatitude jet region. The countercurrents are stronger after the double gyre is removed by the Fourier filter, while the striations remain almost the same in strength, scale, and spatial distribution.

2) CHARACTERISTICS OF THE NONSTATIONARY STRIATIONS

Eastward and westward alternating striations are similar in width in the eastern half of the basin. The westward and eastward barotropic striations are also comparable in strengths and have peak velocities of about $5\,\mathrm{cm\,s^{-1}}$. The average width is approximately 160 km for the striations in both boxes 1 and 2. Striations also exist in the westward branches of the double gyre, but they are less coherent and look like patchy zonal stripes.

The striations are vertically coherent. They are clearly visible in all isopycnal layers, and their width does not change with depth. The striations are strongest in the top layer, where their velocity is around $10\,\mathrm{cm\,s^{-1}}$; in the deep layer, it decreases to about $2\,\mathrm{cm\,s^{-1}}$. We shall see in the rest of this section that this weakening of striation strength with depth is explained by weakening eddy trains.

The striations exhibit noticeable low-frequency temporal variability. The Hovmöller diagram of the barotropic zonal velocity of the striations at the central longitude of box 1 shows two properties (Fig. 6a). First, the striation magnitude oscillates in time. Second, the striations drift southward with a speed of $0.4\,\mathrm{cm\,s^{-1}}$. In contrast, the striations in box 2 (figure not shown) have a tendency to drift northward with a speed of $0.6\,\mathrm{cm\,s^{-1}}$. The baroclinic components of the striations have the same properties and are not shown here. The direction of this drift is consistent with the direction of the Sverdrup flow, but the speed is not. In particular, the spatial average of the Sverdrup flows about -0.1 and $0.1\,\mathrm{cm\,s^{-1}}$ in boxes 1 and 2, respectively, and is not adequate to explain the striation drift. As we shall see in the following, the striation drift is instead consistent with the propagation of large-scale linear modes.

Note that a meridional drift of $0.5\,\mathrm{cm\,s^{-1}}$ over the course of 1 yr will result in a meridional displacement of approximately 150 km, which is similar to the striation width. Longer time averages will smear the striations, which explains why the γ parameter peaks at about 1 yr and decreases at longer times.

b. *Origin of nonstationary striations*

Similar to the flow in the channel, eddies in the double-gyre flow tend to propagate as eddy trains that coincide with the striations. However, because of the

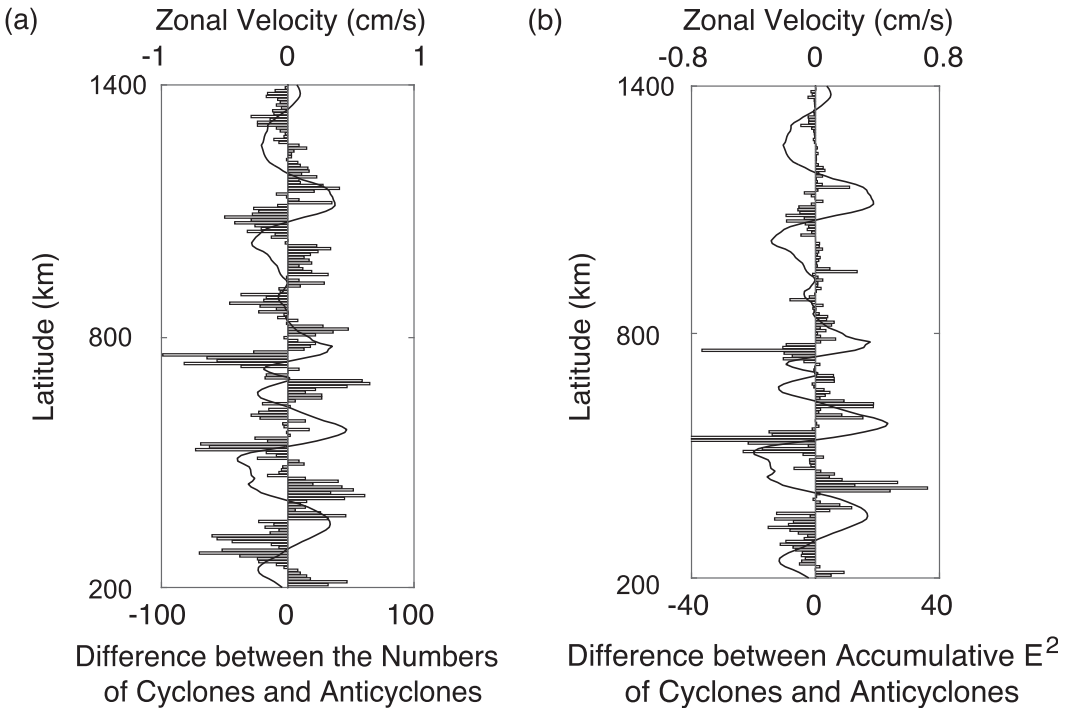

FIG. 7. (a) The difference in the total number of cyclonic and anticyclonic eddies propagating across the striped region shown in Fig. 5b within 1 yr. (b) As in (a), but for the time-integrated E^2 parameter. The black curves are the zonal mean of the zonal velocity of 1-yr mean striations within the striped region.

meridional drift of these striations, their relationship with eddy trains requires more careful examination. Figure 6b shows the Hovmöller diagram of the eddies at the central longitude of box 1. The change in the sign of E^2 with latitude suggests that cyclonic and anticyclonic eddies emerge at alternate latitude bands. The maximum zonal velocity of the drifting striations (Fig. 6a) is located exactly between these cyclonic and anticyclonic eddies, suggesting that the coherent eddies straddle the striations as in the channel model. The E^2 parameter in this diagram shows discontinuous structures in time because of the intermittent presence of coherent eddies in the eddy trains and the fact that E^2 only represents the cores of coherent eddies (Fig. 6b).

The latitudinal variations of both time-averaged $\overline{E^2}$ and the number of cyclonic and anticyclonic eddies further confirm the existence of eddy trains. Figure 7a shows the difference in the number of cyclonic and anticyclonic eddies within the 300-km longitude band (striped area in Fig. 5b) as a function of latitude. The bar graphs exhibit an oscillating pattern, indicating the alternating preferred paths of cyclonic and anticyclonic eddies and a 90° phase shift from the maximum zonal velocity of the striations (the black curve in Fig. 7a). As expected, $\overline{E^2}$ shows a similarly close relationship (Fig. 7b).

The eddy trains are highly correlated with and contribute significantly to the striations. The time-averaged, two-dimensional correlation between u_{eddy} and u_{total} is 0.86 with a CI of 0.01, and the time-averaged spatial correlation between the zonal averages of the two velocities is 0.95 with a CI of 0.01. The u_{eddy} corresponds to 42.8% of u_{total} with a CI of 0.7%, which suggests a significant contribution of eddies to striations. The results for the flow in box 2 are almost the same and consistent with the results from the channel model, as shown in Table 1.

The eddy trains and striations tend to drift at the same speed. As illustrated in Fig. 4b, the cyclonic and anticyclonic eddies emerge at alternating latitudes that are paths of eddy trains and move westward. Subsequent eddies in box 1 (box 2) emerge at more southern (northern) latitudes relative to eddies that emerged at earlier times. In other words, the latitude, at which the eddies within the same eddy train cross a fixed longitude, moves southward (northward) in the subtropical (subpolar) regions, and the speed at which this latitude moves is the drifting speed of the eddy trains. Note also that because this meridional drift is sufficiently slow, several eddies are observed within the same, nearly zonal eddy train at any given moment in time, which makes the definition of an eddy train

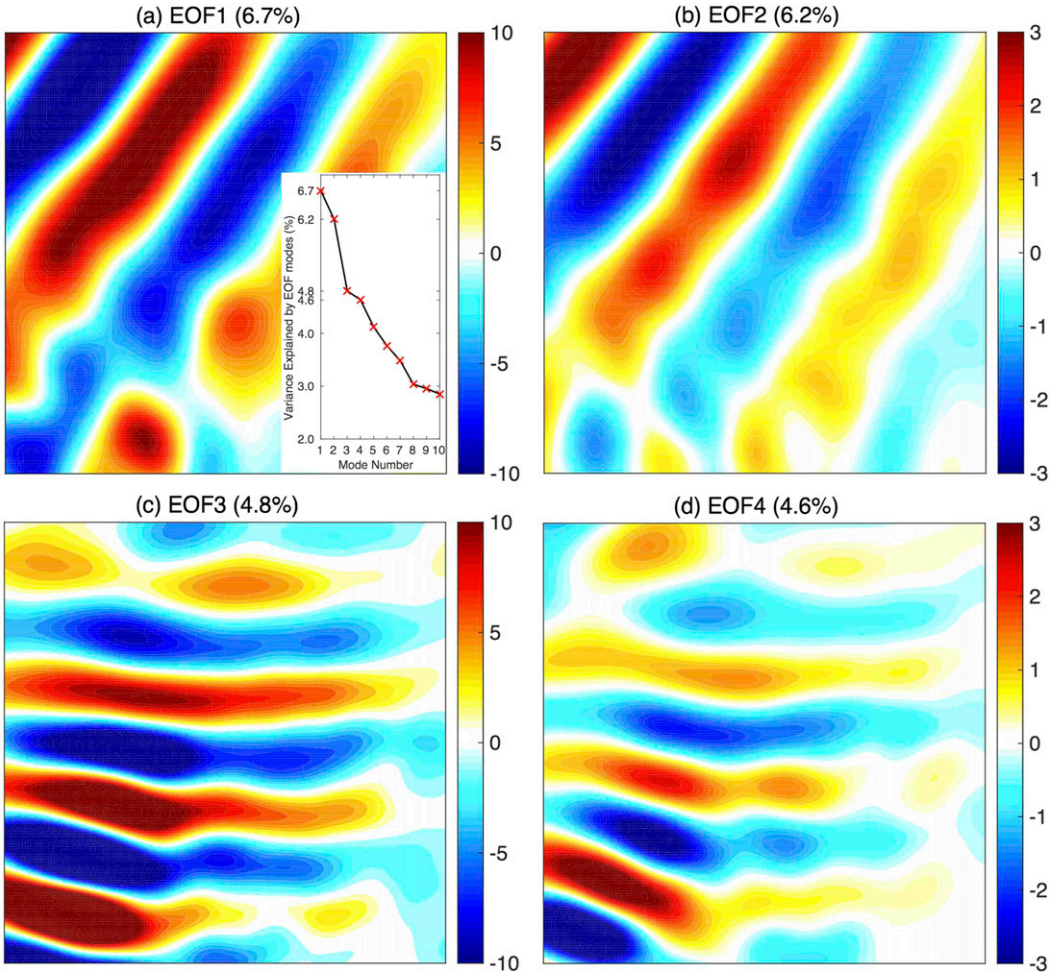

FIG. 8. Reconstructed streamfunction ($m^2\,s^{-1}$) from (a) the first EOF (6.7%), (b) the second EOF (6.2%), (c) the third EOF (4.8%), and (d) the fourth EOF (4.6%) modes of the 20-yr, monthly mean, double-gyre flow within box 1 (denoted in Fig. 5b). The inset in (a) shows the percentage of the flow variance explained by the EOF modes.

meaningful. The drift speed of the eddy trains is equal to that of the striations as discussed in section 4a (Fig. 6).

If the drifting eddy trains correspond to a significant spatially coherent mode of variability, they should be detectable by EOF analysis. EOF-based methods are proven to be effective in studying low-frequency variability of the ocean circulation (e.g., Kondrashov and Berloff 2015). We next calculate the EOFs of the monthly mean barotropic streamfunction within box 1 from the 20-yr model run. Monthly averages are needed to reduce the high-frequency variability; note that an eddy propagating with a speed of $5\,cm\,s^{-1}$ will travel over only 130 km—not sufficient to result in spurious striations. The third and fourth EOF modes (4.8% and 4.6% of the variance) have the shape of zonally elongated striations (Fig. 8), whose width is approximately equal to that of the striations from spatiotemporal filtering (Figs. 5b,c). These paired, phase-shifted EOF modes indicate meridional propagation of the signal. In contrast, the first two EOF modes (6.7% and 6.2% of the variance) have slanted alternating bands and most likely correspond to propagating Rossby waves (e.g., Farrar 2011). EOF modes higher than four do not resemble eddies or striations. The situation in box 2 is qualitatively similar (not shown).

The exact origins of the drift remain unclear, but we propose that it is consistent with the propagation of linear waves in the background flow. To demonstrate this we compare the meridional drift speed of the eddy trains in box 1 with the meridional phase speed of linear modes, whose wavenumbers correspond to those of the zonal striations ($k = 0$ and $l = 7.2 \times 10^{-6}\,m^{-1}$; Figs. 5b,c, 8) for the dynamics linearized around the time-mean flow and under the local homogeneity

assumption. To calculate the phase speed of the linear modes, we use parameters corresponding to the model-simulated time-mean circulation, which is surface intensified, with the area-averaged circulation in the top layer within box 1 being predominantly meridional with a speed of $-1.5\,\mathrm{cm\,s^{-1}}$ (see appendix). Using Eq. (A9), we get a meridional phase speed of the linear mode of about $-0.3\,\mathrm{cm\,s^{-1}}$, which is close to the drifting speed of the striations and eddy trains. A similar agreement applies to the flow in box 2. These results suggest that drifting eddy trains can be related to propagating linear patterns that can develop on these patterns. For example, LaCasce and Pedlosky (2004) showed that the long baroclinic Rossby waves are unstable at all wave amplitudes and that this instability leads to the development of mesoscale eddies that propagate with these waves.

To summarize, the drifting low-frequency striations are manifestations of eddy trains, and these two patterns are closely spatially correlated. It is highly unlikely that these results can be explained by randomly propagating eddies, considering the large number of eddies that systematically propagate within each eddy train. We further explore this distinction in the following section by using a kinematic model of synthetic flows with isolated vortices.

c. A kinematic model of eddy trains

Our main objective here is to explore how one can distinguish between two scenarios: random eddies versus well-organized eddy trains (Fig. 4). Eddies propagate nearly zonally in both cases, and averaging over finite times is not sufficient to make the distinction because time-averaged random eddies can look like striations (Schlax and Chelton 2008), whereas the long-term time average smears all transient structures. The key difference between the two scenarios is in the position of eddy trajectories. In the case of random eddies, the trajectories are distributed randomly in the meridional direction. In the case of eddy trains, a large number of eddies and the corresponding velocity variance are concentrated along zonal tracks; these tracks represent a well-defined mode of variability, and this mode can be readily detected by the EOF analysis. With our kinematic model, we will further show that only eddy trains and not the random eddies can explain the properties of striations and corresponding EOFs in the double-gyre model and altimetry data. The null hypothesis of random eddies, therefore, needs to be rejected.

We carry out two experiments: eddy trains (Expt1) and random eddies (Expt2). Expt1 corresponds to a flow with eddy trains, where multiple cyclones/anticyclones propagate along alternating, nearly zonal tracks. Expt2 illustrates a situation with purely random eddies, where each eddy propagates along its own path.

TABLE 2. Characteristics of eddies in the kinematic model. All parameters are dimensionless.

Eddy parameters	Expt1: Eddy trains	Expt2: Random eddies
λ (day)$^{-1}$	$\mathcal{N}(1.85, 0.09)$[a]	$\mathcal{N}(1.85, 0.09)$
L (km)	$\mathcal{N}(30, 0.3)$	$\mathcal{N}(30, 0.3)$
φ_0 (m^2 s^{-1})	$\mathcal{N}(6.25, 0.125)$	$\mathcal{N}(6.25, 0.125)$
C_x (cm s^{-1})	$\mathcal{U}(9.9, 10.1)$[b]	$\mathcal{U}(9.9, 10.1)$
C_y (cm s^{-1})	$\mathcal{U}(0.495, 0.505)$	$\mathcal{U}(0.495, 0.505)$
x_0 (km)	$\mathcal{U}(0, 960)$	$\mathcal{U}(0, 960)$
y_0 (km)	$\mathcal{N}(y_i^c, 8)$	$\mathcal{U}(0, 960)$

[a] Normal distribution $\mathcal{N}(\mu, \sigma^2)$, where μ is the mean and σ is the variance.
[b] Uniform distribution $\mathcal{U}(a, b)$, where a and b are its minimum and maximum values.
[c] See text in section 4c for description of y_i.

In the experiments, the eddies are described by

$$\varphi = \varphi_0 e^{-\lambda t} e^{\{-[x-(x_0-C_x t)]^2-[y-(y_0-C_y t)]^2\}/2L^2}, \qquad (9)$$

where φ_0 is the initial amplitude, λ is the decay rate, t is the time, L is the eddy radius. The terms x_0 and y_0 are the initial zonal and meridional positions, and C_x and C_y are the zonal and meridional propagating speeds. Following the characteristics of mesoscale eddies described in Chelton et al. (2011) and our analysis of the double-gyre simulation, zonal propagating speeds of the described eddies are westward, while meridional speeds of cyclonic (anticyclonic) eddies are northward (southward) and $C_x/C_y = 0.05$. A detailed description of the parameters is given in Table 2.

In both experiments at any given point in time, there are three cyclonic eddies and three anticyclonic eddies propagating in the model domain, which has a size of $L_x = L_y = 960$ km. Once an eddy exits the domain, a new eddy emerges at (x_0, y_0). The only difference in the two experiments is in the definition of y_0. In Expt1, y_0 follows a normal distribution around the axes of eddy trains, which shifts southward with time, thus generating southward-drifting eddy trains, while in Expt2, y_0 follows a uniform random distribution and generates random eddies. Both experiments are run for a total time of 60 yr.

A short summary of the results from Expt1 and Expt2 is given in Table 3. Expt1 shares many features with the full, double-gyre simulation. Based on the γ parameter, the time average of the instantaneous flow over 70 weeks yields the most robust alternating zonal striations (Fig. 9b). Long-term means do not show distinct striations due to the nonstationary nature

TABLE 3. Flows from two scenarios of propagating eddies.

	Time average	EOF modes
Expt1: Eddy trains	Zonal striations	Modes of variation show drifting striations.
Expt2: Random eddies	Zonal striations	No mode of variation shows striations.

of the striations. We vary the duration of the experiment and find that EOF modes of striations only become visible for model runs longer than 120 weeks, which corresponds to the passing of approximately 80 eddies.

The first two leading EOF modes of the 60-yr model run (4.1% and 3.7% of the variance; Figs. 9c,d) show striations, whereas higher modes do not. The phase shift in space between the two EOF modes indicates meridional drift of the striations. The zonal asymmetry in the striations (Figs. 9b–d) is due to x_0 being normally distributed and C_x being westward, so that more eddies are found in the western part of the domain. Moreover, the Hovmöller diagram of the striations at $x = L_x/2$ shows that the striations migrate southward (figure not shown) with the speed of 0.076 cm s^{-1}, which is about the same as the meridional drifting speed of the eddy trains, 0.077 cm s^{-1}.

In Expt2, westward-propagating random eddies leave zonal tracks in finite-time averages, which resemble striations from the eddy trains case (Fig. 10b). This scenario is similar to that in Schlax and Chelton (2008). The EOF modes, however, consist of cyclonic and anticyclonic vortices but do not exhibit striations (Figs. 10c,d). Therefore, we conclude that the EOF analysis can successfully distinguish eddy trains from spurious striations associated with random eddies and reject the null hypothesis of random eddies. This is because the flow variance in eddy trains is concentrated along predetermined, drifting zonal lines.

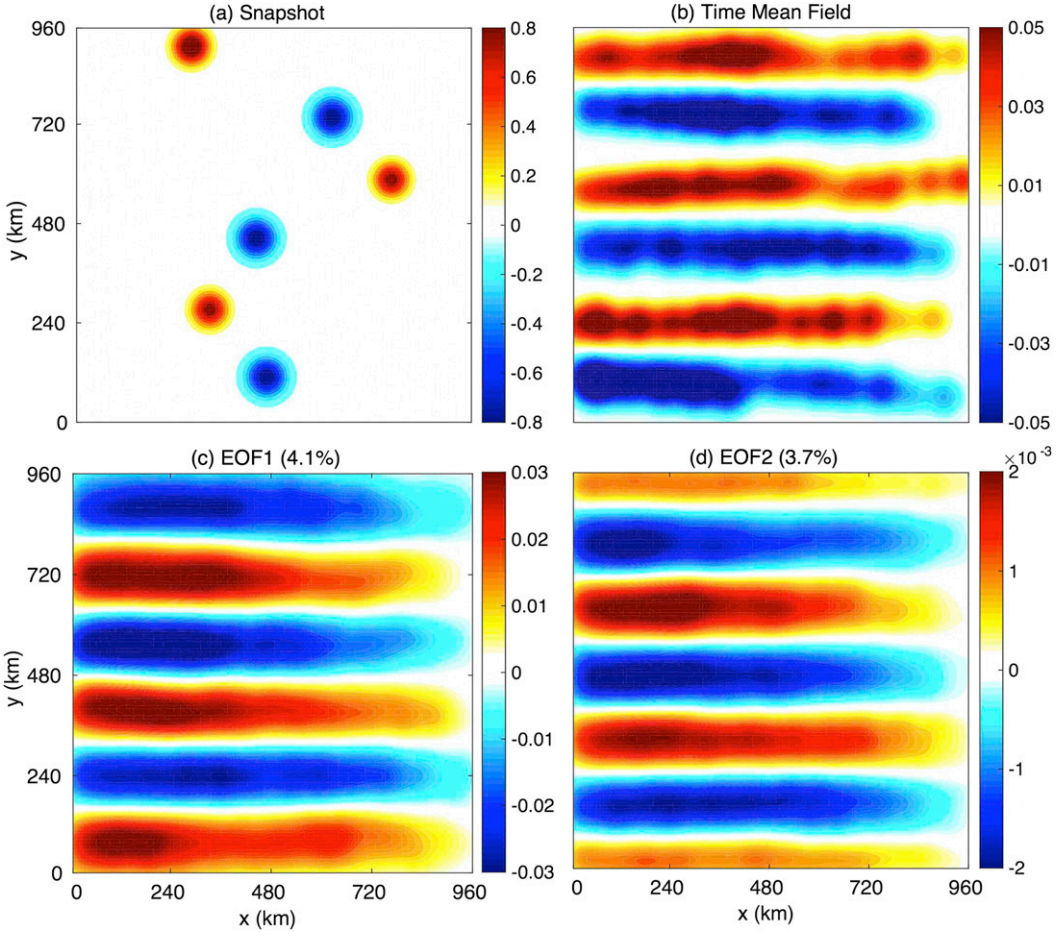

FIG. 9. Eddies and flows in the eddy trains experiment (Expt1) as shown in streamfunction ($m^2\ s^{-1}$). (a) Snapshot of eddies propagating westward around the tracks of zonally oriented eddy trains. (b) Striations as shown by a 70-week mean flow. Striations reconstructed from the (c) first and (d) second EOF modes of the flow.

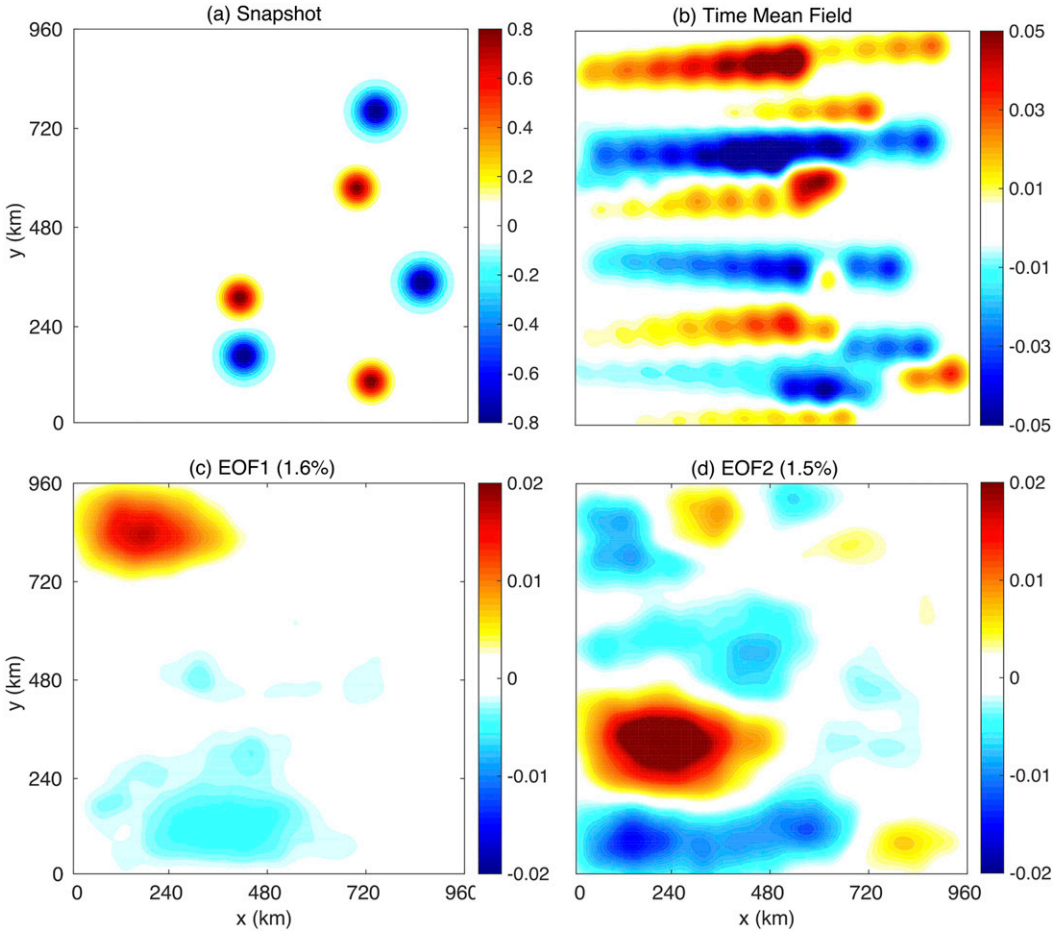

FIG. 10. As in Fig. 9, but for the random eddies experiment (Expt2).

In conclusion, only eddy trains correspond to EOFs in the shape of zonal striations, while the EOFs for random eddies are in the shape of isolated vortices. Averaging over very long periods of time can detect stationary striations by sorting out random eddies from the nonrandom ones; however, it cannot detect drifting striations and is not suitable for this study. EOF analysis can achieve this goal. Recall that our EOF analysis of the monthly mean flows within box 1 of the double-gyre model also shows striations. Therefore, the striations from the double-gyre model are associated with eddy trains. Furthermore, the meridional drifting of the striations can be explained by the drifting eddy trains.

5. Eddy trains in altimetry data

In this section, we examine the relevance of the results from the idealized models to the real ocean and illustrate the concept of eddy trains on the example of the North Pacific. This region is chosen because it allows us to study elongated striations in the basin interior, away from the boundaries and strong boundary currents. As in the model analysis, we compare striations in the low-pass filtered SLA data with the EOF analysis of the same data. Note that we do not attempt to examine stationary jets or striations in the mean dynamic topography (MDT) fields because they were studied before (Maximenko et al. 2008; Maximenko et al. 2009), are not simulated by our double-gyre, QG model, and cannot be revealed by the EOF analysis.

The striations extend hundreds of kilometers in the zonal direction (Fig. 11a), making the random eddies interpretation unlikely. Visual inspection of eddy paths estimated by E^2 suggests that eddies propagate along well-defined zonal tracks as eddy trains and these tracks correspond to the striations. As determined by γ, 16 months is a proper time scale for detecting the striations. The resulting striations are nonstationary and

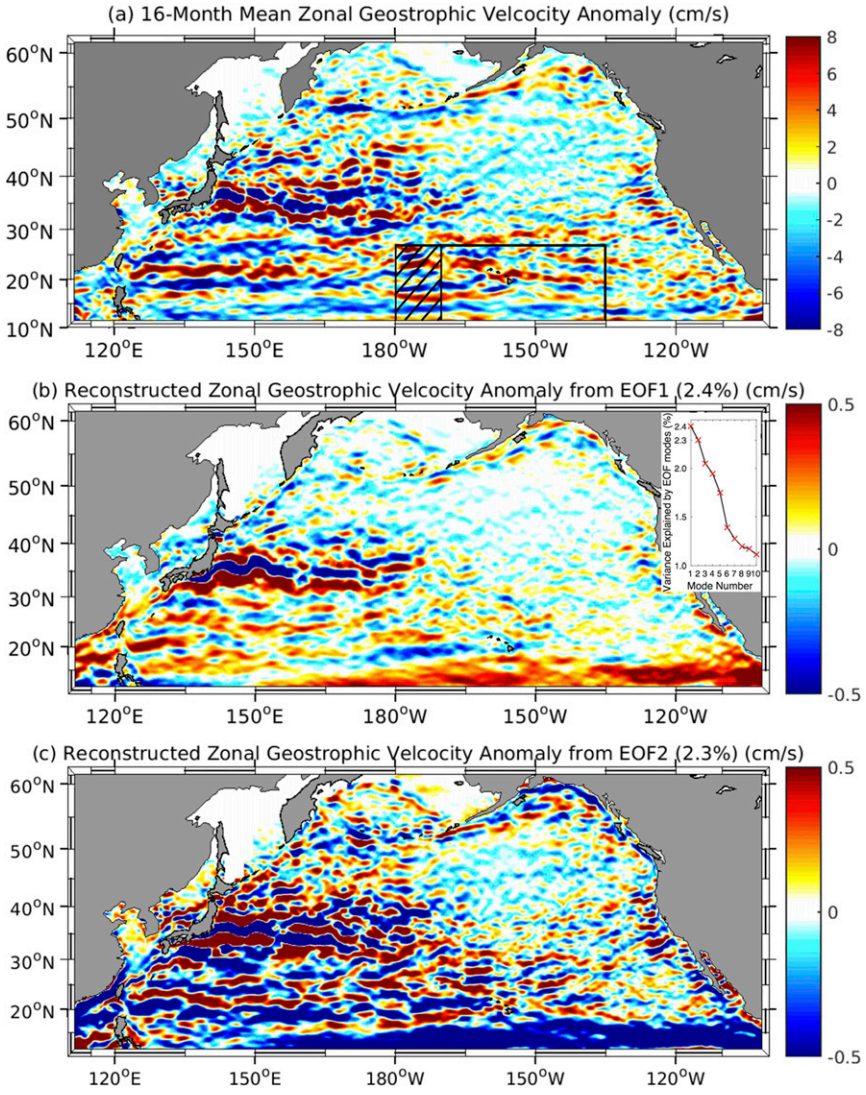

FIG. 11. Striations in the North Pacific Ocean. (a) A 16-month mean of zonal geostrophic velocity anomaly. The flows within the black box and the striped region are selected to study eddy and striation properties (see text). (b) Zonal geostrophic velocity anomaly reconstructed from the first EOF mode (2.4%). The inset shows the percentage of the flow variance explained by the EOF modes. (c) As in (b), but for the second EOF mode (2.3%).

have different zonal scales and strengths. We focus on the southeastern region (rectangular box in Fig. 11a).

Visual inspection of propagating eddies within the longitude band (10° to 27°N and 180° to 170°W) marked by the striped box in Fig. 11a reveals that multiple eddies that propagate along the same latitudes are organized into eddy trains. As in the case of the double-gyre model, we use several methods of quantifying the relationship between eddy trains and striations. The numbers of cyclonic and anticyclonic eddies crossing the longitude band (Fig. 12a) have distinct maxima and minima, and they are 90° phase shifted relative to the zonal velocity of the striations; time-averaged E^2 reveals a similar picture (Fig. 12b). The zonal velocity of the striations and the corresponding E^2 parameter are strongly spatially correlated (with a 90° phase shift) with a coefficient of 0.81, and this value is statistically significant within the box region. The correlation between the two-dimensional u_{eddy} and u_{total} is about 0.87 with a CI of 0.001. The mean correlation between the zonally averaged u_{eddy} and u_{total} is 0.92 with a CI of 0.002. Finally, the velocity contribution from the eddy cores u_{eddy} contributes to 42.3% of u_{total} with a CI of 0.1%.

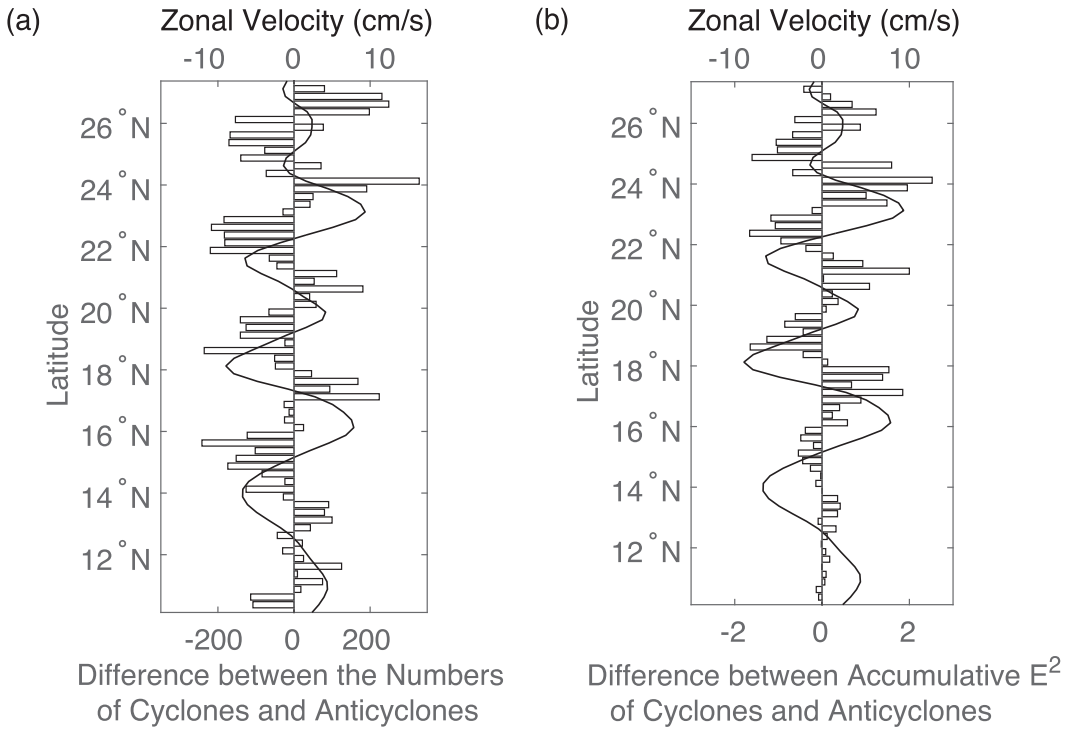

FIG. 12. (a) The difference in the total number of cyclonic and anticyclonic eddies propagating across the striped region shown in Fig. 10a within 16 months. (b) As in (a), but for the time-integrated E^2 parameter. The black curves are the zonal mean of the zonal velocity of 16-month mean striations within the striped region.

Last, we employ EOF analysis of the daily snapshots of geostrophic zonal velocity anomalies and find that the first two EOF modes (2.4% and 2.3% of the variance) are in the form of zonal striations (Figs. 11b,c), which are consistent with the eddy trains. These elongated EOF patterns illustrate a tendency of multiple eddies to propagate along the same eddy tracks, and EOF analysis distinguishes this situation from idealized random eddies. These paired EOF modes also indicate propagation, and the eddy trains and striations in the North Pacific tend to drift meridionally away from the intergyre boundary. This drift is similar to that in the double-gyre model. Striations within the subtropical gyre, approximately from 10° to 40°N, tend to drift southward, while striations within the subpolar gyre are much weaker and have no distinguishable drift (Fig. 13a). The directions of the drifting eddy trains (represented by the E^2 parameter) and striations in the subtropical gyre are in good agreement with each other (Fig. 13b).

6. Discussion and conclusions

This study explores the relationship between eddies and multiple striations in a broad, eastward-flowing, QG current, a double-gyre QG flow, and altimetry data in the North Pacific. The results consistently show that a large number of coherent eddies propagate along nearly zonal paths, and we refer to these strings of eddies as eddy trains. The eddy trains are dominated by either cyclonic or anticyclonic eddies at alternate latitudes, and time averages of these eddy trains lead to striations in zonal velocity. Based on our E^2 parameter for identifying the cores of coherent eddies, most of the striation velocity is explained by that from eddy trains. We therefore conclude that these striations can be interpreted as signatures of time-averaged eddy trains.

In the eastward-flowing, QG current, eddies tend to propagate as eddy trains along fixed, zonal paths. These stationary eddy trains are clearly visible as zonal striations (or zonal jets) in the long-term averages of the flow. C. Chen et al. (2015) further showed that the paths of eddies tend to follow f/H contours when meridional ridges are introduced into the bottom of the channel. In contrast, in the wind-driven, double gyres and altimetry data, eddy trains are nonstationary and slowly drift meridionally, away from the intergyre boundary. Consequently, low-pass filtered velocities exhibit drifting striations, and the eddy trains and striations drift together, maintaining a close spatial correlation. This drift, however, complicates the detection of zonal striations in long-term averages, and our analysis shows that EOF analysis is a better alternative to spatiotemporal filtering.

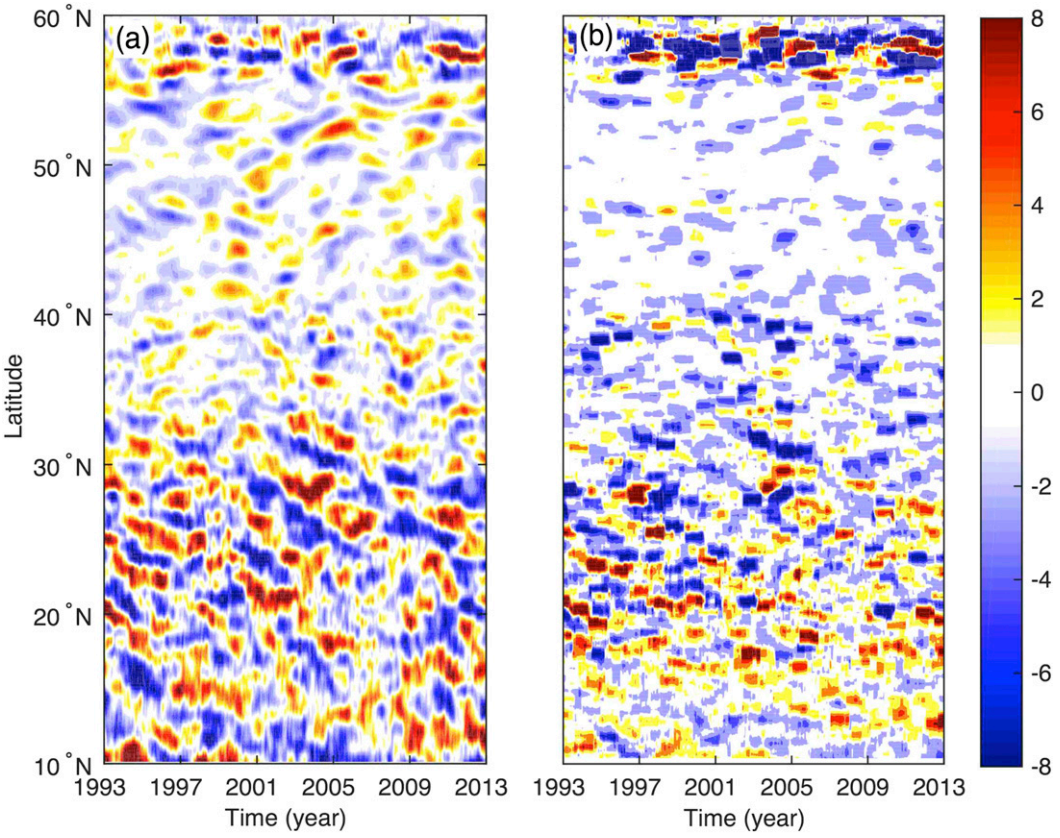

FIG. 13. Meridional drift of the striations in the North Pacific Ocean. (a) Hovmöller diagrams of the low-pass filtered (16-month running mean) zonal velocity of the striations (cm s^{-1}) and (b) of the corresponding E^2 parameter (10^{-12} s^{-2}) at 148°W.

The reported relationship between eddy trains and striations can be contrasted with two other possible interpretations of the observed striations: coherent zonal jets that are hidden behind strong but chaotic eddy fields and as artifacts of averaging of spatially uncorrelated, zonally propagating eddies. The reported persistent tendency of eddies to propagate within eddy trains contradicts both of these scenarios. The migrating eddy trains are analogous to storm tracks, observed in Earth's atmosphere and the ACC (Bischoff and Thompson 2014).

The results suggest that most, if not all, transient striations are explained by eddy trains. However, it is still possible that more realistic flows, such as our double-gyre flow and real ocean circulations, contain vortices that straddle zonal jets and thus only partly contribute to striations. The estimate of eddy contribution to the striations depends on the method of identifying eddy boundaries, which is a challenging task (e.g., Beron-Vera et al. 2013; Wu 2014; Faghmous et al. 2015; Wang et al. 2015). For example, Buckingham and Cornillon (2013) showed that eddies detected by a contour identification method account for 30%–70% of the velocity variance of striations. Our E^2-based estimate of less than 50% provides only a lower bound for vortex contribution to striations, since E^2 is a measure of the vortex core only. Note also that the E^2 parameter can only identify strong coherent eddies and does not account for other types of mesoscale currents.

Eddy trains aligned in the meridional direction represent a large-scale template for eddy propagation. The existence of this pattern may be explained by linear dynamics. LaCasce and Pedlosky (2004) showed that the long, baroclinic Rossby waves are unstable at all wave amplitudes and that this instability contributes to the midlatitude eddies that develop on these waves. Berloff and Kamenkovich (2013a, b) also suggested that linear results can predict the properties of nonlinear mesoscale eddies and describe most of the mesoscale eddies as a wave turbulence phenomenon. Our own analysis suggests that linear modes in the appropriate background flow propagate with the same meridional phase speed as the eddy trains. It is, therefore, likely that the observed eddy trains and linear modes are strongly correlated and tied by mutual feedbacks, thus constituting one dynamical entity. Identification and quantification of

these feedbacks are beyond the scope of this paper and should be a subject of future studies.

Our results can potentially improve parameterizations of eddy-induced material transport. For example, we expect that the eddy trains and striations can lead to a highly anisotropic, predominantly zonal material transport (Kamenkovich et al. 2009a), which is not currently accounted for in climate models. Our conclusions do not imply that all eddies move within eddy trains, and isolated and nonzonally propagating eddies are certainly possible (e.g., Chelton et al. 2011). Findings of the paper have to be extended to and verified in much more turbulent and eddy-resolving flow regimes, like the ones achieved by Shevchenko and Berloff (2015).

Acknowledgments. This study was supported by the National Science Foundation Grant OCE-1154923. P. Berloff gratefully acknowledges the support of this work by the NERC Grant NE/J006602/1.

APPENDIX

The Dispersion Relation of a Three-Layer QG Model with a Vertically Sheared Meridional Current

We consider a three-layer, QG model on the β plane. Potential vorticity q_n in the three layers is governed by

$$\frac{\partial q_n}{\partial t} + J(\psi_n, q_n) = 0 \quad (n = 1,2,3), \tag{A1}$$

where the layer index starts from the top, and ψ_n is the streamfunction in the nth layer. The PVs q_n are

$$\begin{aligned} q_n = {} & \nabla^2\psi_n + \beta_0 y + \delta_{n1}F_1(\psi_2 - \psi_1) \\ & + \delta_{n2}[F_{21}(\psi_1 - \psi_2) + F_{22}(\psi_3 - \psi_2)] \\ & + \delta_{n3}F_3(\psi_2 - \psi_3). \end{aligned} \tag{A2}$$

We decompose ψ_n into the background part ϕ_n and streamfunction disturbances φ_n:

$$\psi_n = \phi_n + \varphi_n. \tag{A3}$$

We are interested in the baroclinicity of a large-scale meridional ocean current with a vertical shear and consider a horizontally uniform flow V in the upper layer and motionless lower layers:

$$\phi_1 = Vx, \quad \phi_2 = 0, \quad \phi_3 = 0. \tag{A4}$$

The governing equations can be rewritten as

$$\begin{aligned} \frac{\partial\zeta_1}{\partial t} + J(\varphi_1,\zeta_1) + \beta\frac{\partial\varphi_1}{\partial x} + F_1V\frac{\partial\varphi_1}{\partial y} + \left(\beta + \frac{\partial\zeta_1}{\partial y}\right)V = 0, \\ \frac{\partial\zeta_2}{\partial t} + J(\varphi_2,\zeta_2) + \beta\frac{\partial\varphi_2}{\partial x} - F_{21}V\frac{\partial\varphi_2}{\partial y} = 0, \\ \frac{\partial\zeta_3}{\partial t} + J(\varphi_3,\zeta_3) + \beta\frac{\partial\varphi_3}{\partial x} = 0, \end{aligned} \tag{A5}$$

where ζ_n are PV perturbation anomalies and

$$\begin{aligned} \zeta_n = {} & \nabla^2\varphi_n + \delta_{n1}F_1(\varphi_2 - \varphi_1) + \delta_{n2}[F_{21}(\varphi_1 - \varphi_2) \\ & + F_{22}(\varphi_3 - \varphi_2)] + \delta_{n3}F_3(\varphi_2 - \varphi_3). \end{aligned} \tag{A6}$$

Linearizing the equations around V, we obtain

$$\begin{aligned} \left(\frac{\partial}{\partial t} + V\frac{\partial}{\partial y}\right)\zeta_1 + \left(\beta\frac{\partial}{\partial x} + F_1V\frac{\partial}{\partial y}\right)\varphi_1 = 0, \\ \frac{\partial\zeta_2}{\partial t} + \left(\beta\frac{\partial}{\partial x} - F_{21}V\frac{\partial}{\partial y}\right)\varphi_2 = 0, \\ \frac{\partial\zeta_3}{\partial t} + \beta\frac{\partial\varphi_3}{\partial x} = 0. \end{aligned} \tag{A7}$$

The normal-mode solutions can be sought in the form $\varphi_n = A_n e^{i(kx+ly-\omega t)}$, which upon substitution into Eq. (A7) yields three coupled algebraic equations for A_1, A_2, and A_3:

$$\begin{aligned} & [(Vl-\omega)(k^2+l^2) - \omega F_1 - \beta k]A_1 + (\omega - Vl)F_1A_2 = 0, \\ & \omega F_{21}A_1 + [(Vl-\omega)F_{21} \\ & \quad - \omega(k^2+l^2) - \omega F_{22} - \beta k]A_2 + \omega F_{22}A_3 = 0, \\ & \omega F_3A_2 - [\omega F_3 + \omega(k^2+l^2) + \beta k]A_3 = 0. \end{aligned} \tag{A8}$$

Nontrivial solutions for A_1, A_2, and A_3 exist only if the determinant of the coefficients is zero. This leads to the dispersion relation:

$$\begin{vmatrix} (Vl-\omega)(k^2+l^2) - \omega F_1 - \beta k & (\omega - Vl)F_1 & 0 \\ \omega F_{21} & (Vl-\omega)F_{21} - \omega(k^2+l^2) - \omega F_{22} - \beta k & \omega F_{22} \\ 0 & -\omega F_3 & \omega F_3 + \omega(k^2+l^2) + \beta k \end{vmatrix} = 0. \tag{A9}$$

REFERENCES

Baldwin, M. P., P. B. Rhines, H.-P. Huang, and M. E. McIntyre, 2007: The jet-stream conundrum. *Science*, **315**, 467–468, doi:10.1126/science.1131375.

Berloff, P., 2015: Dynamically consistent parameterization of mesoscale eddies. Part I: Simple model. *Ocean Modell.*, **87**, 1–19, doi:10.1016/j.ocemod.2014.12.008.

——, and I. Kamenkovich, 2013a: On spectral analysis of mesoscale eddies. Part I: Linear analysis. *J. Phys. Oceanogr.*, **43**, 2505–2527, doi:10.1175/JPO-D-12-0232.1.

——, and ——, 2013b: On spectral analysis of mesoscale eddies. Part II: Nonlinear analysis. *J. Phys. Oceanogr.*, **43**, 2528–2544, doi:10.1175/JPO-D-12-0233.1.

——, ——, and J. Pedlosky, 2009: A mechanism of formation of multiple zonal jets in the oceans. *J. Fluid Mech.*, **628**, 395–425, doi:10.1017/S0022112009006375.

——, S. Karabasov, J. T. Farrar, and I. Kamenkovich, 2011: On latency of multiple zonal jets in the oceans. *J. Fluid Mech.*, **686**, 534–567, doi:10.1017/jfm.2011.345.

Beron-Vera, F. J., Y. Wang, and M. J. Olascoaga, 2013: Objective detection of oceanic eddies and the Agulhas leakage. *J. Phys. Oceanogr.*, **43**, 1426–1438, doi:10.1175/JPO-D-12-0171.1.

Bischoff, T., and A. F. Thompson, 2014: Configuration of a Southern Ocean storm track. *J. Phys. Oceanogr.*, **44**, 3072–3078, doi:10.1175/JPO-D-14-0062.1.

Boland, E. J. D., A. F. Thompson, E. Shuckburgh, and P. H. Haynes, 2012: The formation of nonzonal jets over sloped topography. *J. Phys. Oceanogr.*, **42**, 1635–1651, doi:10.1175/JPO-D-11-0152.1.

Buckingham, C. E., and P. C. Cornillon, 2013: The contribution of eddies to striations in absolute dynamic topography. *J. Geophys. Res. Oceans*, **118**, 448–461, doi:10.1029/2012JC008231.

——, ——, F. Schloesser, and K. M. Obenour, 2014: Global observations of quasi-zonal bands in microwave sea surface temperature. *J. Geophys. Res. Oceans*, **119**, 4840–4866, doi:10.1002/2014JC010088.

Chelton, D. B., M. G. Schlax, and R. M. Samelson, 2011: Global observations of nonlinear mesoscale eddies. *Prog. Oceanogr.*, **91**, 167–216, doi:10.1016/j.pocean.2011.01.002.

Chen, C., I. Kamenkovich, and P. Berloff, 2015: On the dynamics of flows induced by topographic ridges. *J. Phys. Oceanogr.*, **45**, 927–940, doi:10.1175/JPO-D-14-0143.1.

Chen, R., and G. R. Flierl, 2015: The contribution of striations to the eddy energy budget and mixing: Diagnostic frameworks and results in a quasigeostrophic barotropic system with mean flow. *J. Phys. Oceanogr.*, **45**, 2095–2113, doi:10.1175/JPO-D-14-0199.1.

——, ——, and C. Wunsch, 2015: Quantifying and interpreting striations in a subtropical gyre: A spectral perspective. *J. Phys. Oceanogr.*, **45**, 387–406, doi:10.1175/JPO-D-14-0038.1.

Faghmous, J. H., I. Frenger, Y. Yao, R. Warmka, A. Lindell, and V. Kumar, 2015: A daily global mesoscale ocean eddy dataset from satellite altimetry. *Sci. Data*, **2**, 150028, doi:10.1038/sdata.2015.28.

Farrar, J. T., 2011: Barotropic Rossby waves radiating from tropical instability waves in the Pacific Ocean. *J. Phys. Oceanogr.*, **41**, 1160–1181, doi:10.1175/2011JPO4547.1.

Huang, H.-P., A. Kaplan, E. N. Curchitser, and N. A. Maximenko, 2007: The degree of anisotropy for mid-ocean currents from satellite observations and an eddy-permitting model simulation. *J. Geophys. Res.*, **112**, C09005, doi:10.1029/2007JC004105.

Kamenkovich, I., P. Berloff, and J. Pedlosky, 2009a: Anisotropic material transport by eddies and eddy-driven currents in a model of the North Atlantic. *J. Phys. Oceanogr.*, **39**, 3162–3175, doi:10.1175/2009JPO4239.1.

——, ——, and ——, 2009b: Role of eddy forcing in the dynamics of multiple zonal jets in a model of the North Atlantic. *J. Phys. Oceanogr.*, **39**, 1361–1379, doi:10.1175/2008JPO4096.1.

——, I. Rypina, and P. Berloff, 2015: Properties and origins of the anisotropic eddy-induced transport in the North Atlantic. *J. Phys. Oceanogr.*, **45**, 778–791, doi:10.1175/JPO-D-14-0164.1.

Karabasov, S. A., and V. M. Goloviznin, 2009: Compact accurately boundary-adjusting high-resolution technique for fluid dynamics. *J. Comput. Phys.*, **228**, 7426–7451, doi:10.1016/j.jcp.2009.06.037.

——, P. S. Berloff, and V. M. Goloviznin, 2009: CABARET in the ocean gyres. *J. Ocean Modell.*, **30**, 155–168, doi:10.1016/j.ocemod.2009.06.009.

Kondrashov, D., and P. S. Berloff, 2015: Stochastic modeling of decadal variability in ocean gyres. *Geophys. Res. Lett.*, **42**, 1543–1553, doi:10.1002/2014GL062871.

Kondratyev, K., and G. Hunt, 1982: *Weather and Climate on Planets.* Elsevier, 768 pp.

LaCasce, J. H., and J. Pedlosky, 2004: The instability of Rossby basin modes and the oceanic eddy field. *J. Phys. Oceanogr.*, **34**, 2027–2041, doi:10.1175/1520-0485(2004)034<2027:TIORBM>2.0.CO;2.

Maximenko, N. A., B. Bang, and H. Sasaki, 2005: Observational evidence of alternating zonal jets in the World Ocean. *Geophys. Res. Lett.*, **32**, L12607, doi:10.1029/2005GL022728.

——, O. V. Melnichenko, P. P. Niiler, and H. Sasaki, 2008: Stationary mesoscale jet-like features in the ocean. *Geophys. Res. Lett.*, **35**, L08603, doi:10.1029/2008GL033267.

——, P. Niiler, L. Centurioni, M.-H. Rio, O. Melnichenko, D. Chambers, V. Zlotnicki, and B. Galperin, 2009: Mean dynamic topography of the ocean derived from satellite and drifting buoy data using three different techniques. *J. Atmos. Oceanic Technol.*, **26**, 1910–1919, doi:10.1175/2009JTECHO672.1.

Nadiga, B. T., 2006: On zonal jets in oceans. *Geophys. Res. Lett.*, **33**, L10601, doi:10.1029/2006GL025865.

Okubo, A., 1970: Horizontal dispersion of floatable particles in the vicinity of velocity singularities such as convergences. *Deep-Sea Res. Oceanogr. Abstr.*, **17**, 445–454, doi:10.1016/0011-7471(70)90059-8.

O'Reilly, C. H., A. Czaja, and J. H. LaCasce, 2012: The emergence of zonal ocean jets under large-scale stochastic wind forcing. *Geophys. Res. Lett.*, **39**, L11606, doi:10.1029/2012GL051684.

Pedlosky, J., 1987: *Geophysical Fluid Dynamics*. 2nd ed. Springer-Verlag, 710 pp.

Richards, K. J., N. A. Maximenko, F. O. Bryan, and H. Sasaki, 2006: Zonal jets in the Pacific Ocean. *Geophys. Res. Lett.*, **33**, L03605, doi:10.1029/2005GL024645.

Schlax, M. G., and D. B. Chelton, 2008: The influence of mesoscale eddies on the detection of quasi-zonal jets in the ocean. *Geophys. Res. Lett.*, **35**, L24602, doi:10.1029/2008GL035998.

Shepherd, T. G., 1990: *Topological Fluid Mechanics.* Cambridge University Press, 278–287.

Shevchenko, I. V., and P. S. Berloff, 2015: Multi-layer quasi-geostrophic ocean dynamics in Eddy-resolving regimes. *Ocean Modell.*, **94**, 1–14, doi:10.1016/j.ocemod.2015.07.018.

Tanaka, Y., and K. Akitomo, 2010: Alternating zonal flows in a two-layer wind-driven ocean. *J. Oceanogr.*, **66**, 475–487, doi:10.1007/s10872-010-0040-x.

Wang, Y., M. J. Olascoaga, and F. J. Beron-Vera, 2015: Coherent water transport across the South Atlantic. *Geophys. Res. Lett.*, **42**, 4072–4079, doi:10.1002/2015GL064089.

Weiss, J., 1991: The dynamics of enstrophy transfer in two-dimensional hydrodynamics. *Physica D*, **48**, 273–294, doi:10.1016/0167-2789(91)90088-Q.

Wu, Q., 2014: Region-shrinking: A hybrid segmentation technique for isolating continuous features, the case of oceanic eddy detection. *Remote Sens. Environ.*, **153**, 90–98, doi:10.1016/j.rse.2014.07.026.